Highly Stable Luminous "Snakes" from $CsPbX_3$ Perovskite Nanocrystals Anchored on Amine-Coated Silica Nanowires

Aizhao Pan,[†] Matthew J. Jurow,[‡,#] Youshen Wu,[†] Mengjun Jia,[†] Fuyin Zheng,[$] Yanfeng Zhang,[†] Ling He,[,†] and Yi Liu[*,‡,#]*

†Department of Chemistry, School of Science, Xi'an Jiaotong University, Xianning West Road, 28, Xi'an, 710049, China.

‡The Molecular Foundry, #Materials Sciences Division, Lawrence Berkeley National Laboratory, Berkeley, California 94720, United States.

$Department of Materials Science and Engineering, Massachusetts Institute of Technology, Cambridge, MA 02139, United States.

Corresponding Author

*Email: heling@mail.xjtu.edu.cn

*Email: yliu@lbl.gov

KEYWORDS assembled hierarchical membrane, colloidal $CsPbX_3$ nanocrystal, photostability, serpentine silica nanowires, superhydrophobic

ABSTRACT

Despite the exceptional optoelectronic characteristics of perovskite nanocrystals (NCs), the materials' potential applications are primarily limited by their instability arising from the ionic nature of the $CsPbX_3$ (X=Cl, Br and I) lattice, low formation energy and spontaneous ion exchange. Herein, we introduce a facile and effective *in-situ* growing strategy to prepare extremely stable composites (abbr. $CsPbX_3$@CA-SiO_2) by anchoring $CsPbX_3$ NCs onto silica nanowires (NWs), which effectively depresses the optical degradation of their photoluminescence (PL) and enhances stability. The serpentine silica NWs, with tunable lengths of up to 8 μm, are prepared by anisotropic *sol-gel* growth of hydrolyzed tetraethylorthosilicate (TEOS) with 3-aminopropyltriethoxysilane (APTES) and trimethoxy(octadecyl)silane (TMODS) in a water/oil emulsion. The free amino groups are employed as surface ligands for growing perovskite NCs, yielding distributed monodisperse NCs (~8 nm) around the NW matrix. The emission wavelength is tunable by simple variation of the halide compositions ($CsPbX_3$, X=Cl, Br or I) and the composites demonstrate a high photoluminescence quantum yield (PLQY 32-69%). Additionally, we have demonstrated the composites $CsPbX_3$@CA-SiO_2 can be self-woven to form a porous 3D hierarchical NWs membrane, giving rise to a superhydrophobic surface with hierarchical micro/nano structural features. Most importantly, the resulting composites exhibit remarkable chemical stability towards water, and much enhanced photostability and thermal stability. This work presents an effective strategy to incorporate perovskite NCs onto functional matrices as multifunctional stable light sources.

Introduction

All inorganic colloidal perovskite nanocrystals in the form of $CsPbX_3$ (X = Cl, Br or I) have seen a burst of attention in recent years because of their exceptional photophysical properties and optoelectonic applications.[1-3] $CsPbX_3$ NCs exhibit near unity quantum yields without explicit shelling, narrow line widths, and bandgaps tunable over the whole visible spectral range,[3-6] which may allow them to rival or even exceed traditional semiconductor nanocrystals for a wide range of optoelectronic applications including light-emitting diodes (LED), lasers, photodetectors, solar cells and display backlights.[7-10]

Currently, the applications of $CsPbX_3$ perovskite NCs are limited by the materials' instability towards moisture, heat, UV light and chemicals, especially halides.[11-15] The instability originates from the low formation energy of $CsPbX_3$ NCs, and the ligand lability imparted by the ionic nature of the $CsPbX_3$ lattice.[11, 16-18] In most cases, exposure to moisture or polar solvents causes energy shifting, luminescent peak broadening, severe PL quenching and unacceptably short device lifetimes.[17, 19-22] Color purity and stability are also deteriorated by facile halide anion-exchange reactions, from which mixed-anion $CsPb(X/Y)_3$ (X/Y =Cl, Br or I) NCs are created.[4, 23]

Recent efforts to improve perovskite NCs stability are well reviewed, but are far from satisfying. Generally, regulating surface ligands is an effective approach to improve stability, including the introduction of long-chain, branched or sterically hindered surfactants, which serve as capping ligands to create surface passivation layers around the NCs.[11, 24-28] Typically, branched (3-aminopropyl) triethoxysilane (APTES),[29] sterically demanding polyhedral oligomeric silsesquioxane (POSS),[30] polydentate chelates,[31]or alkyl phosphate[32] have been employed as passivation layers to yield high stability perovskite NCs.

Incorporating or embedding NCs into a protective matrix, such as inorganic materials (SiO_2, zeolite-Y, MOF, phospho-silicate glass, etc.) or polymers is another effective strategy to improve stability.[33-39] Incorporating $CsPbX_3$ NCs into various hydrophobic matrices, such as polystyrene (PS),[18, 37, 40] PVP/silicone resin,[41] POSS-based copolymers[15] with chemically addressable ligands,[15, 25] or the diblock copolymer PS-*b*-PVP [42] can preserve well-defined morphology and bright fluorescence, while dramatically enhancing the NCs' stability towards UV light and water. Additionally, the $CsPbBr_3$ NCs can be also confined in Zeolite-Y,[35] silica,[28, 38] ammonium bromide,[43] or onto the surfaces of amine-mediated monodisperse silica[36] to provide a physical barrier for water permeation, and effectively suppress the optical and water-induced degradation of their photoluminescence (PL). Beyond those, surface self-passivation has been also shown as an effective option to stabilize the $CsPbBr_3$ NCs.[44, 45]

Scheme 1. Schematic illustration of the *in-situ* formation strategy and growing process of $CsPbBr_3$@CA-SiO_2 composites (a and b). As grown, the SiO_2 nanowires feature ligands with exposed amine groups that anchor the growth of $CsPbBr_3$ NCs. Schematic structures of the as-

prepared 3D luminous "snake" of $CsPbBr_3$@CA-SiO_2 composites (c and d)

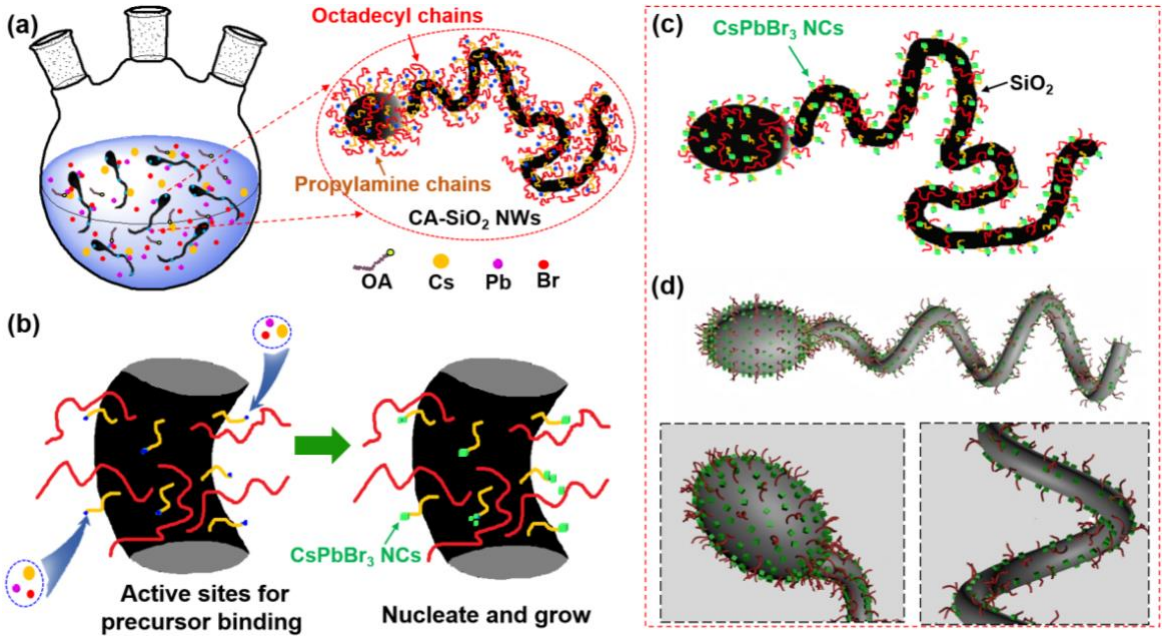

Herein, we have developed composites with $CsPbBr_3$ NCs grown *in-situ* onto octadecyl/propylamine capped SiO_2 nanowires (**Scheme 1**). These materials have well-defined morphology, outstanding optical properties and excellent stabilities. Templating the growth in this way 1) inhibits NC sintering,[36] 2) provides a layer of long octadecyl chains that improves hydrophobicity, and 3) allows for assembly into an exceptionally stable and superhydrophobic porous 3D hierarchical membrane of NWs.

We first demonstrated the successful preparation of functionalized silica nanowires by anisotropic deposition of hydrolyzed TEOS, APTES and TMODS. The $CsPbBr_3$ NCs can then be grown onto the functionalized NWs in under 5 minutes. The emission wavelength of the composite can be easily tuned throughout the visible region by controlling the anion composition. The resulting composites exhibit extraordinary stability towards water and enhanced photostability. These composites can be further assembled into porous, super-hydrophobic 3D hierarchical membranes. This work presents an effective strategy for the *in situ* growth of perovskite NCs onto

chemically functionalized matrices, opening the door to a library of stable perovskite-based composites.

Results and discussion

Perovskite nanocrystals are typically synthesized in the presence of amine or carboxyl terminated ligands.[1, 3] These functionalities preferentially coordinate with precursors to form nucleation and adsorption sites, which contribute to the homogenization of NCs (Scheme 1b).[28, 33, 42] Here we replaced the common small molecule ligands with octadecyl/propylamine capped silica NWs, fabricated by hydrolysis and condensation of TEOS, APTES and TMODS.

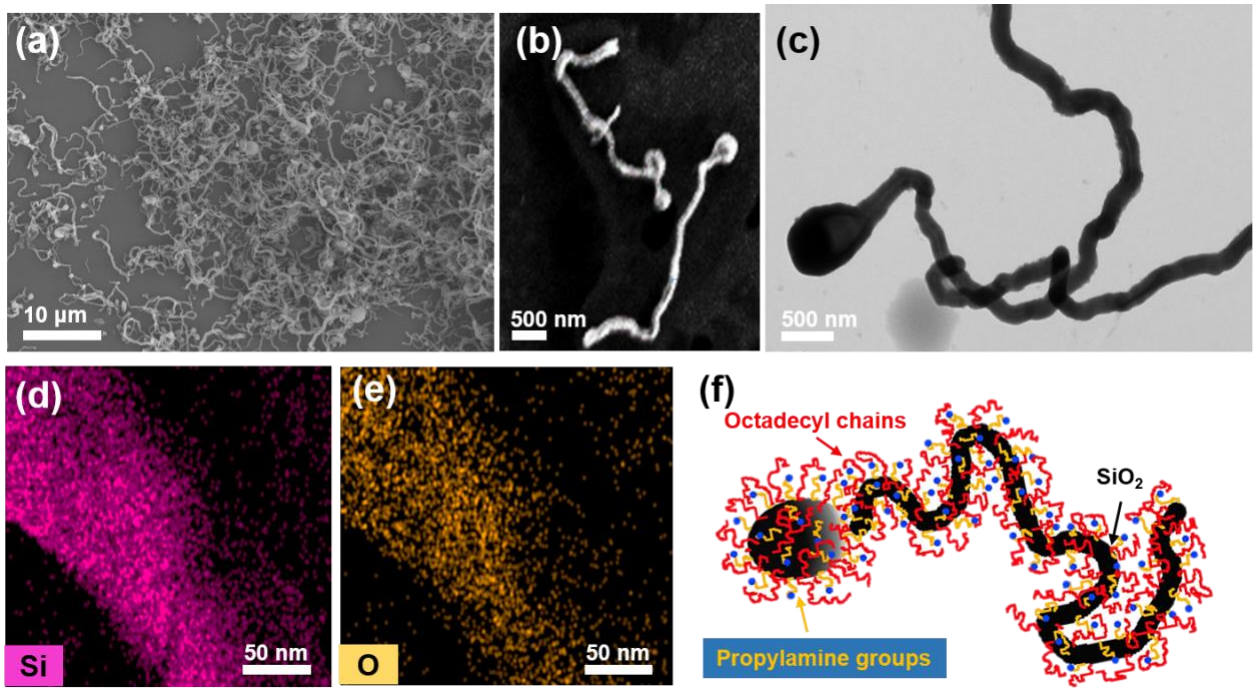

Figure 1. Morphologies of octadecyl/propylamine capped silica (CA-SiO_2) NWs. SEM images from concentrated (a) and highly diluted (b) CA-SiO_2 NWs. (c) TEM image of CA-SiO_2 NWs. (d and e) Elemental mapping profiles of Si (d) and O (e) elements. (f) The schematic drawing of the octadecyl/propylamine capped silica NWs.

Figure 1 shows SEM images of the octadecyl/propylamine capped silica NWs (abbr. CA-SiO_2 NWs) which have a well-defined snake-like shape, with a bulky spherical head (ca. 500 nm in diameter) and a slender body (ca. 120 nm in diameter and 5-10 μm in length). The long silica NWs remain intact even after 1 hour of vigorous sonication, demonstrating the NWs' excellent flexibility and durability (Figure 1b and c). Control experiments were conducted using TEOS and APTES precursors to afford propylamine capped silica NWs (A-SiO_2) or TEOS and TMODS precursors to afford octadecyl capped silica NWs (C-SiO_2). NWs with very different aspect ratios were thus obtained. A-SiO_2 NWs have bigger heads, with diameters around 500 nm-2 μm and body lengths of around 200 nm. C-SiO_2 NWs feature heads apprxoimately 400 nm in diameter and a 120 nm-long body (Figure S1). EDS mapping images of oxygen (O) and silicon (Si) of C-SiO_2 NWs demonstrate that the octadecyl/propylamine capped groups are distributed across the whole NW (Figure 1d and e). A schematic drawing of the CA-SiO_2 NWs is depicted in Figure 1f, simulating the shape of a "snake" with a bulky head and a slim body capped with octadecyl and propylamine groups.

Surface composition of the silica NWs was characterized using Fourier Transform infrared (FTIR) spectroscopy and high-resolution X-ray photoelectron spectroscopy (XPS) analysis (Figure S2). The strong peaks in the FTIR at 1100 cm^{-1} and 800 cm^{-1} are assigned to the asymmetric stretching vibration, and deformation vibration of Si-O-Si. The peaks at 2850 cm^{-1} and 2925 cm^{-1} are ascribed to symmetric and asymmetric stretching vibrations of -CH_2- and -CH_3 respectively, with those at 1465 cm^{-1} and 1380 cm^{-1} assigned to symmetric bending vibrations of the same functionalities. The peaks at 3450 cm^{-1} and 1560 cm^{-1} in the FTIR spectra of CA-SiO_2 and A-SiO_2 NWs are assigned to the stretching and deformation vibration of NH_2 groups. XPS studies confirm the chemical elemental compositions of the capped silica NWs (Figure S2b). The

peaks of CA-SiO_2 NWs at 102.79 eV, 531.61 eV, 401.88 eV and 284.82 eV are assigned to the binding energies of Si2p, O1s, N1s and C1s, respectively, while the N1s peak is absent in the XPS spectrum of C-SiO_2 NWs. The collective results confirm the specific morphology and surface compositions of CA-SiO_2 NWs, which render them a viable matrix for nanoparticle anchoring.[29, 36]

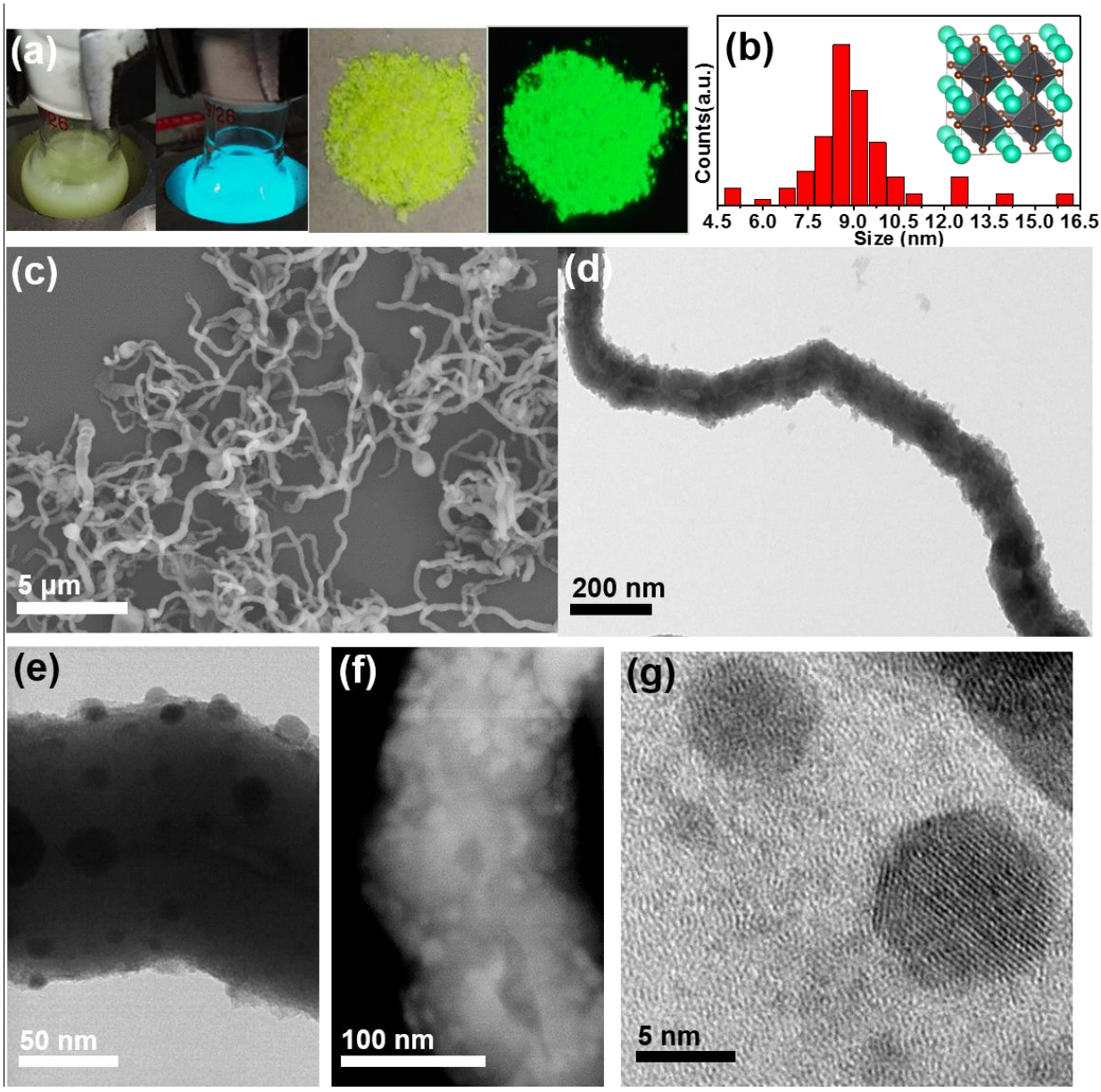

Figure 2. Morphologies and structures of the $CsPbBr_3$@CA-SiO_2 composite. (a) Digital images of the as-synthesized composite in solution and the corresponding powder under daylight and UV

light. (b) Size distribution of the loaded $CsPbBr_3$ NCs on SiO_2 NWs. The inset is a schematic image of the crystal structure of $CsPbBr_3$. SEM (c) and TEM (d) images of $CsPbBr_3$@CA-SiO_2 composite. The magnified TEM (e), STEM (f) and HR-TEM (g) images of the typical morphology of $CsPbBr_3$@CA-SiO_2 composite.

We tracked the growth of the NCs on the composite $CsPbBr_3$@CA-SiO_2 "snakes" by watching the fluorescent variations of the intermediate products. As the reaction progresses, the transparent solution begins to turn turbid chartreuse with deep blue emission under UV light. Blue and bright cyan emission can be observed (Figure S3) after 2 and 4 min, respectively. The solution emits bright green light after 5 min, after which no further red shift is observed (snapshots in Figure 2a). The resulting powder of $CsPbBr_3$@CA-SiO_2 also shows strong PL intensity under UV light (Figure 2a), similar to the strong emission of free $CsPbBr_3$ NCs.[3, 5]

The proposed growth process is illustrated in Scheme 1. The exposed amine functionalities on the SiO_2 NW ligands facilitate the uptake of the NC precursors by coordinating with lead halides and Cs^+ to form nucleation sites, at which perovskite nanocrystals grow to give the well-defined and highly luminescent $CsPbBr_3$@CA-SiO_2 composite.[33, 42] Stray dissociated oleylamine helps to bind perovskite precursors onto the CA-SiO_2 NWs, generating monodisperse, evenly distributed NCs. Free ligand is then easily removed by centrifuge during subsequent purification. No unbound NCs are observed in the SEM image of the final luminescent composites (Figure 2c). Compared with the smooth surface of CA-SiO_2 NWs (Figure S4), NCs are observed to uniformly adhere and distribute on the surface of silica NWs in the $CsPbX_3$@CA-SiO_2 samples by TEM (Figure 2d and 2e and S4b). The average size of the NCs is 8-10 nm (Figure 2b). Well-structured NCs can also be observed by STEM images (Figure 2f).

The crystallinity of $CsPbX_3$@CA-SiO_2 is clearly verified by high-resolution TEM (HR-TEM) in Figure 2g, corresponding to the typical crystal lattice planes of $CsPbBr_3$. Further sampling by

TEM and STEM at different locations shows that the morphology is consistent with the formation of $CsPbX_3$@CA-SiO_2 (Figure S5). In comparison, samples from physically mixed C-SiO_2 NWs and $CsPbBr_3$ (abbr. $CsPbBr_3$/C-SiO_2) show weakly bounded NWs and NCs with clear phase separation (Figure S6). Taken together, the microscopy and spectroscopy confirm the synthesis of 3D luminous snake-shaped composites of $CsPbX_3$@CA-SiO_2 with distributed $CsPbX_3$ NCs on the SiO_2 NWs matrix, as illustrated in Scheme 1.

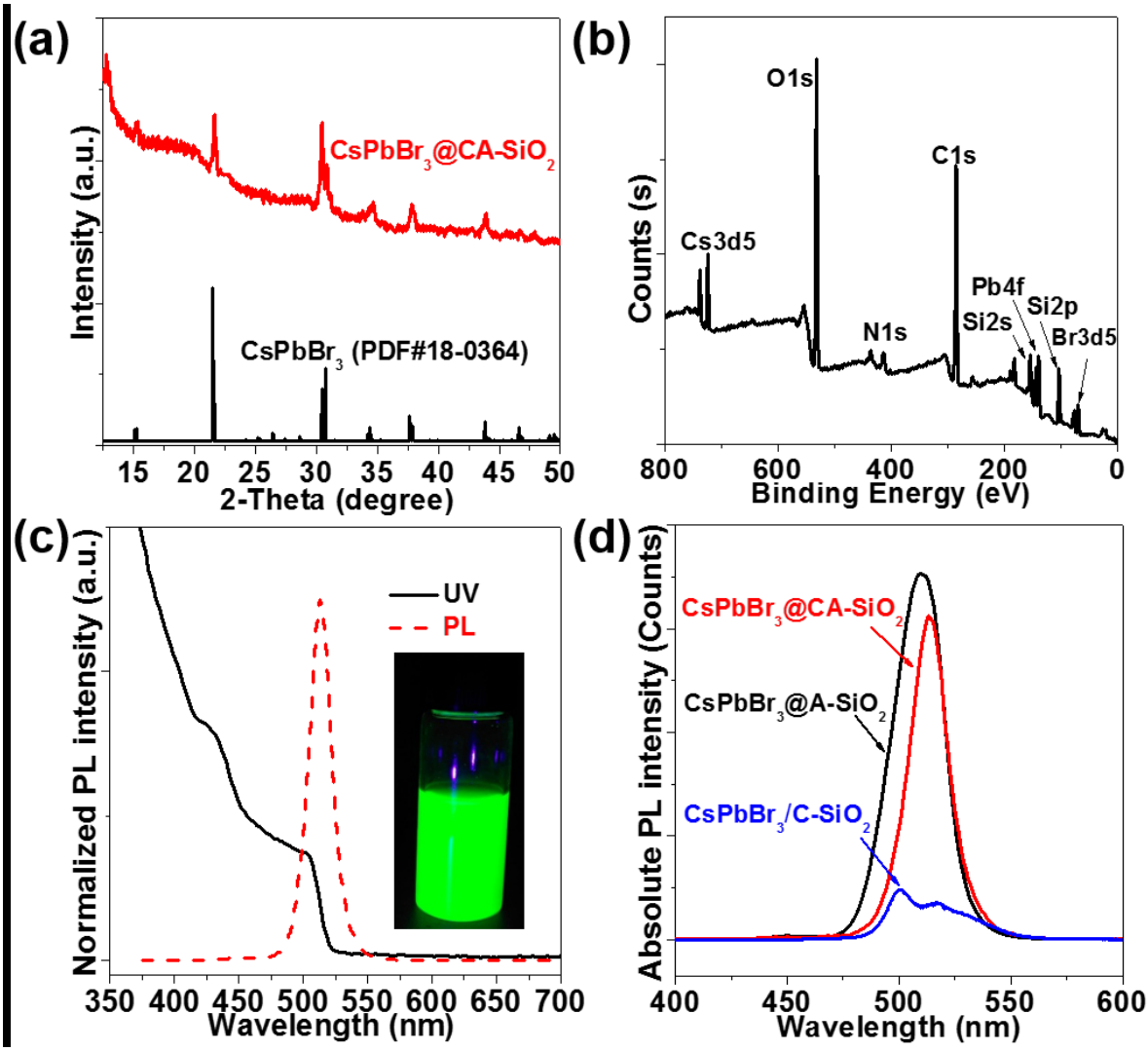

Figure 3. Chemical structure and optical properties of $CsPbBr_3$@CA-SiO_2 composites. (a) XRD pattern of $CsPbBr_3$@CA-SiO_2 powder overlayed withthe standard orthorhombic crystal structure of $CsPbBr_3$. (b) High-resolution X-ray photoelectron spectra (XPS) analysis of $CsPbBr_3$@CA-

SiO_2 powder with a survey scan. (c) Optical absorption and PL emission spectra of $CsPbBr_3$@CA-SiO_2. Insets: (c) is a photograph of the colloidal solution in toluene under UV light; (d) Photoluminescence spectra of the composites of $CsPbBr_3$@A-SiO_2, $CsPbBr_3$/C-SiO_2 and $CsPbBr_3$@CA-SiO_2.

Further structural details of the $CsPbBr_3$@CA-SiO_2 composite are provided by powder X-ray diffraction pattern (PXRD), high-resolution X-ray photoelectron spectra (XPS) and energy dispersive spectrometer (SEM-EDS) analysis in Figure 3. The PXRD patterns of the $CsPbBr_3$@CA-SiO_2 powders show bragg peaks at 2θ=17.6, 25.1, 35.6, 39.6, 43.5, 50.2, 53.2 and 56.2° in the diffractogram, consistent with the orthorhombic crystal phase (JCPDF #01-072-7929) of $CsPbBr_3$ (Figure 3a).[3, 5] XPS elemental composition analysis of $CsPbBr_3$@CA-SiO_2 powder (Figure 3b, and Figure S7) further confirms that the composite powder contains all the elements expected from the $CsPbBr_3$ NCs and surface ligands. The elemental ratio for Cs:Pb:Br measured by XPS amounts to 1:1:3.1, which matches well with the expected stoichiometry. The specific elemental composition of Si, Cs, Pb and Br of the $CsPbBr_3$@CA-SiO_2 composite is also confirmed by the SEM-EDS spectrum (Figure S8).

The UV-Vis absorption and photoluminescence (PL) spectra of $CsPbBr_3$@CA-SiO_2 show an absorption onset and PL emission peak at 512 nm and 514 nm, respectively, and a PLQY value above 65% (Figure 3c). The PLQY of the $CsPbBr_3$@CA-SiO_2 is higher than that of previously reported encapsulated NCs, such as APTES-/NH_2-POSS-$CH_3NH_3PbBr_3$ (15-55%),[29] QDs@glass (15.6%),[46] POSS-$CsPbBr_3$ (61%),[30] and $CsPbBr_3$@NH_4Br nanocomposite (64.21%).[43] The as-prepared composite of $CsPbBr_3$@CA-SiO_2 shows slightly lower PL intensity than $CsPbBr_3$@A-SiO_2, but much higher PL intensity than $CsPbBr_3$/C-SiO_2 due to the phase separation in the blended sample (Figure 3d and Figure S9).

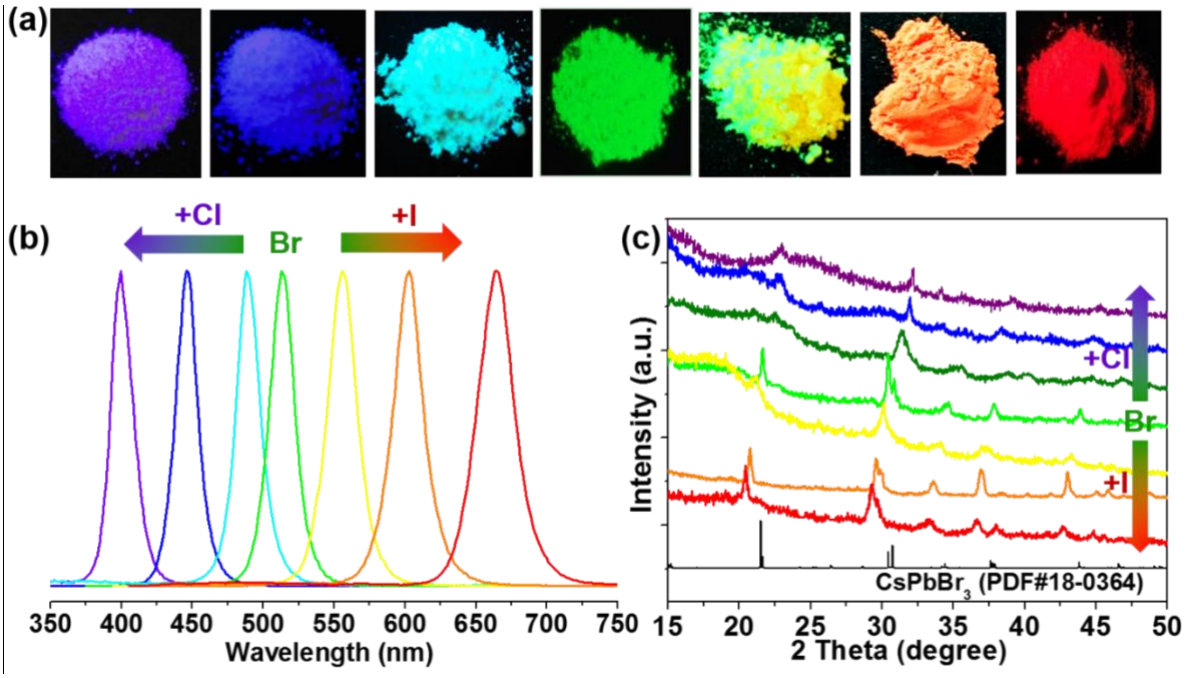

Figure 4. Controllable photoluminescence via anion modulation. (a) Optical images of the corresponding composites under a UV lamp (365 nm) with different emission colors. Photoluminescence spectra (b) and XRD patterns (c) of the as-prepared solid luminophores with various Cl/Br/I ratios.

The band gap of halide perovskites can be easily tuned by anion substitution.[4, 23] Thus, the $CsPbX_3$@CA-SiO_2 composites with various emission colors have been prepared by using different lead halide precursors other than $PbBr_2$ (including pure $PbCl_2$, various mixtures of $PbCl_2$/$PbBr_2$, $PbBr_2$/PbI_2, and pure PbI_2) in the *in-situ* growth process in Figure 4. Figure 4a shows the optical images of the corresponding samples under a UV lamp (365 nm) with different emission colors. Pure bromide samples ($CsPbBr_3$@CA-SiO_2) show green emission (λ_{max} 514 nm, PLQY >65%) and samples with more chloride or iodide show blue-shifted or red-shifted emission (QYs between 30%-62%), respectively (Figure 4b). PXRD patterns demonstrate that all the composites of $CsPbX_3$@CA-SiO_2 crystalize in the orthorhombic perovskite structure (Figure 4c). The slight shift of the diffraction peaks toward the large and small angle direction when chloride and iodide are

introduced is consistent with the formation of the orthorhombic $CsPbCl_3$, $CsPb(Cl/Br)_3$, $CsPb(Br/I)_3$ and $CsPbI_3$ crystal phases.

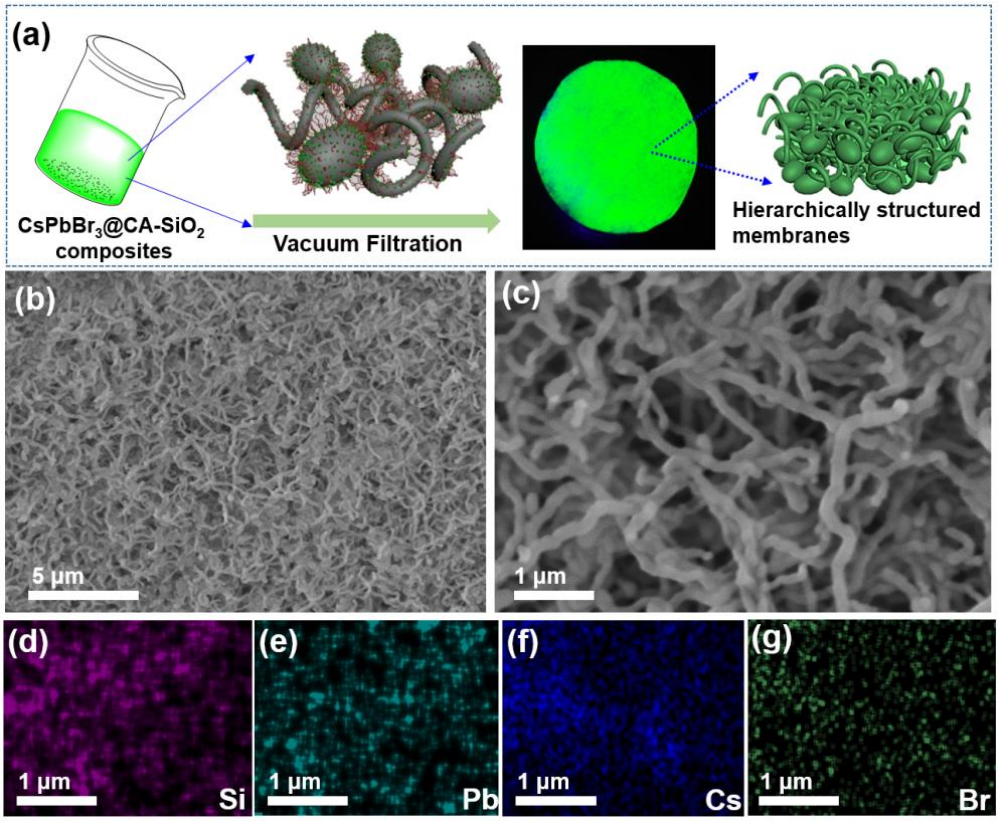

Figure 5. Hierarchically structured membranes assembled from $CsPbBr_3$@CA-SiO_2 composite. (a) Schematic illustration of the $CsPbBr_3$@CA-SiO_2 membrane obtained by vacuum filtration, and the corresponding digital photograph of the membrane. Low (b) and high (c) magnification SEM images of the $CsPbBr_3$@CA-SiO_2 membrane. SEM-elemental mapping profiles of Si (d), Pb (e), Cs (f) and Br (g) of the $CsPbBr_3$@CA-SiO_2 membrane.

The composite can be readily assembled into a compact hierarchically structured porous membrane by vacuum filtration.[47] Membranes were prepared by dropping the $CsPbBr_3$@CA-SiO_2 solution onto a piece of filter paper under continuous vacuum and results in a self-woven membrane tightly attached to the substrate (Figure 5a and S10a). SEM images reveal the formation of a porous membrane made of entangled $CsPbBr_3$@CA-SiO_2 NWs, similar to the ubiquitous ramen noodle (Figure 5b and c), and free of stray perovskite particles. Elemental mapping using

energy dispersive X-ray analyzer (EDX) confirmed the presence of Si, Pb, Cs and Br elements inside the membrane (Figure 5d-g). Further sampling by SEM at different locations proved the consistent morphology of the $CsPbBr_3$@CA-SiO_2 (Figure S10b). Formation of the woven features is not only attributed to the high aspect ratio and flexibility of the long NWs, but also the strong interaction among the capping octadecyl groups on the silica NWs. The as-fabricated hierarchical membrane is composed of microstructured SiO_2, the surface of which is coated with octadecyl/propylamine chains and $CsPbBr_3$ NCs as the secondary nanostructures (Figure 5a), which is expected to endow hydrophobicity while remaining highly luminescent.

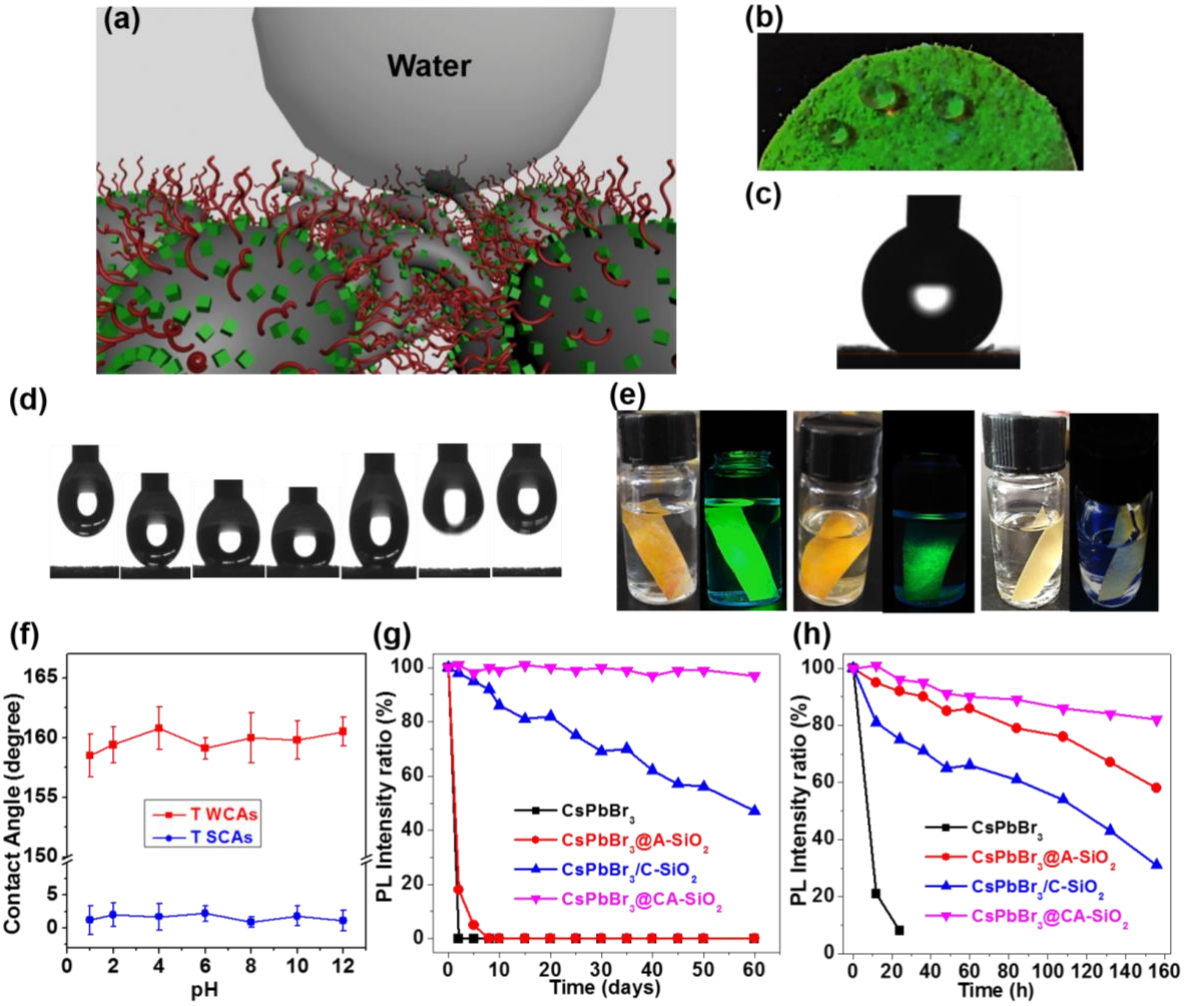

Figure 6. Improved stabilities of the hierarchical membranes relative to normal perovskite NCs. (a) Schematic illustration of the hierarchical membrane assembled from $CsPbBr_3$@CA-SiO_2

composites for enhanced stability and de-wetting property. (b-d) Photos showing the hydrophobicity and de-wetting property of $CsPbBr_3$@CA-SiO_2 membrane. (e) Photographs taken under ambient light or UV irradiation after immersing $CsPbBr_3$@CA-SiO_2, $CsPbBr_3$/C-SiO_2 and $CsPbBr_3$@A-SiO_2 membranes, respectively, in water for 60 days. (f) The variation of water contact angles (CA) on the $CsPbBr_3$@CA-SiO_2 membrane at different pH values. The relative PLQY plots upon immersing in water over time (g) and against different UV irradiation times (h) for $CsPbBr_3$@CA-SiO_2, $CsPbBr_3$@A-SiO_2 and $CsPbBr_3$/C-SiO_2 membranes.

Commonly, perovskite nanocrystals $CsPbX_3$ (X=Cl, Br, I) are easily degraded by ambient humidity, upon contacting with polar solvents or after irradiating by UV light.[12, 19-20] The hierarchically structured membrane from $CsPbBr_3$@CA-SiO_2 was expected to afford enhanced de-wetting properties and environmental stability due to the micro/nano-scale structure of SiO_2 NWs and octadecyl-enriched surface (Figure 6a). As shown in Figure 6b-d, the $CsPbBr_3$@CA-SiO_2 based membrane does show excellent de-wetting and superhydrophobicity, quantified by water contact angle measurement yielding a value of 162°. Resistance to water was quantified by immersing the membrane in deionized water over different periods of time (Figure 6e and g) and was also compared against a variety of control samples. The membrane from $CsPbBr_3$@CA-SiO_2 displayed the best PL stability, with less than 5% PL decay after 60 days of total submersion (Figure 6g). For comparison, the luminescence of $CsPbBr_3$ NCs was quenched completely after immersing in water for 1 hour (Figure S11), while the relative PL of the $CsPbBr_3$@A-SiO_2 membrane decayed to only 18% of its initial value after 2 d. Better PL stability was observed for the membrane of the physically blended $CsPbBr_3$/C-SiO_2. These samples displayed a PL decay of 31% and 53% after immersing in water for 30 days and 60 days, respectively. Impressively, the membranes showed almost identical WCAs and sliding contact angles (SCAs) after immersion in solutions at pHs from 0 to 14, suggesting that the surface morphology is not impacted by acid/base chemistry (Figure 6f).

The hierarchical $CsPbBr_3$@CA-SiO_2 membrane also exhibits enhanced photostability relative to both the neat $CsPbBr_3$ NCs and the colloidal $CsPbBr_3$/C-SiO_2 composites. After 24 h exposure to UV irradiation, no measurable PL intensity decrease was observed (less than 10% decay) for the $CsPbBr_3$@CA-SiO_2 and $CsPbBr_3$@A-SiO_2 membranes, while the PL of the neat $CsPbBr_3$ NCs was severely quenched. The PL of $CsPbBr_3$/C-SiO_2 membrane decayed to 75% and 30% of its initial value after 24 h and 156 h irradiation (Figure 6h). For $CsPbBr_3$@CA-SiO_2, ~81% of the initial PL intensity was still maintained even after 156 h. Notably, no PL peak shift was detected (Figure S12), indicating that the $CsPbBr_3$ NCs remain well separated due to their encapsulation within the surface alkyl layer. The thermal stability was tested by cycling the solid material between 120 °C and room temperature. The as-fabricated $CsPbBr_3$@CA-SiO_2 membrane shows greater retention of its luminescence after 5 cycles (＞82%) when compared to the $CsPbBr_3$ NCs (32%) (Figure S13a). The $CsPbX_3$@CA-SiO_2 membranes remain luminescent, maintaining approximately half of its initial PL intensity even after boiling in water and UV light illumination for 60 s (Figure S13b).Finally, the tendency toward anion exchange is suppressed for the $CsPbBr_3$@CA-SiO_2 membrane, as no emission color change was observed after exposure to a chloride or iodide solution for 24 h at room temperature (Figure S13c), or under UV light illumination (Figure S13d). It should be noted that when the temperature was elevated to 80 ℃, significant PL intensity decrease was observed, accompanied by insignificant peak shifts, which may be related to inferior thermal stability of NCs and slight anion exchange (Figure S13d). Such inertness to anion exchange is held in sharp contrast to that of films of free $CsPbBr_3$ NCs, where dramatic anion-induced color change is observed, again underscoring the stabilization effect endowed by the superhydrophobic surface.

Conclusions

In summary, we report a facile and effective *in-situ* growth strategy for highly luminescent and extremely stable $CsPbX_3$ NCs anchored on silica NWs ($CsPbBr_3$@CA-SiO_2). The silica NWs capped with a layer of mixed octadecyl and propylamine terminated ligands were obtained with a 500 nm head, a tunable body length of up to 8 μm, and a diameter of 120 nm. The free amine end groups were subsequently employed as ligands for perovskite NCs growth, yielding evenly distributed NCs (~8 nm) around the SiO_2 NWs with tunable emission properties. In addition, a vacuum filtration method was used to fabricate $CsPbBr_3$@CA-SiO_2 membranes with a hierarchical micro-nanostructure. The resulting membrane forms a superhydrophobic surface with a high PLQY, remarkable chemical stability towards water, and much enhanced photostability and thermal stability. This work presents an effective strategy for growing perovskite NCs onto functional matrices to form perovskite-based composites, paving the way for future optoelectronic applications.

Experimental Sections

Materials and Chemicals: $PbBr_2$ (99.90%), Cs_2CO_3 (99.99%), octadecene (ODE, 90%), oleic acid (OA, 90%, AR), oleylamine (OLA, 90%, AR), 3-aminopropyl-triethoxysilane (APTES, 99%), tetraethoxysilane (TEOS, >98%), polyvinylpyrrolidone (Mw=24 kDa) and trimethoxy(octadecyl)silane (TMODS, 90%) were purchased from Aladdin and used as received without purification. All the other solvents were used as received without any purification.

Preparation of octadecyl/propylamine capped silica (CA-SiO_2) NWs: The octadecyl/propylamine capped silica (CA-SiO_2) NWs were synthesized following a modified procedure.[47] In a typical synthesis, polyvinylpyrrolidone (1.0 g, Mw=24 kDa) was dissolved in *n*-pentanol (8.0 ml) in a 50 mL centrifugation tube. Then, ethanol (1.0 mL), deionized water (0.28 mL), sodium citrate solution (0.67 mL, 0.18 M in water), and ammonia solution (0.20 mL, NH_3

content 25 wt%) were injected sequentially, and the mixture was shaken by hand for 5 min after each chemical was added. Then, a mixture of 100 μL of TEOS, 15 μL of TMODS and 4 μL APTES (or 6 μL APTES for A-SiO_2 NWs or 15 μL TMODS for C-SiO_2 NWs) was added to the above solution and shaken immediately for 10 min. The solution was left static for 24 h at room temperature. The octadecyl/propylamine capped silica (CA-SiO_2) NWs were then separated by centrifugation and washed with ethanol three times, and finally dispersed in ethanol to form a suspension with a silica concentration of 20 mg/mL.

Synthesis of $CsPbBr_3$@CA-SiO_2: A typical synthesis of $CsPbBr_3$@CA-SiO_2 following a modified procedure is described in Scheme 1.[36] Cs_2CO_3 (0.1 mmol), $PbBr_2$ (0.2 mmol, or equal molar for other lead halide precursors), CA-SiO_2 NWs (0.3 g), ODE (10 mL), oleylamine (0.3 mL), and oleic acid (1 mL) were mixed and heated under vigorous stirring at 125 ℃. In five minutes, the reaction was cooled to room temperature in an ice/water bath, and the reaction mixture was subjected to three to five cycles of centrifugation/re-dispersion in hexane. The resulting composite was dried in a vacuum oven overnight before being stored for future use. The control sample of $CsPbBr_3$@A-SiO_2 was synthesized in a similar fashion, and the control sample of $CsPbX_3$/C-SiO_2 was synthesized by mixing C-SiO_2 with pre-prepared $CsPbX_3$ NCs.[3, 5]

Fabrication of $CsPbBr_3$@CA-SiO_2 NW membrane: A simple vacuum filtration method was developed to fabricate hierarchical $CsPbBr_3$@CA-SiO_2 membrane on substrates. In a typical procedure, 10 mL of a diluted $CsPbBr_3$@CA-SiO_2 suspension (5 mg/mL) in toluene was filtered through a compact filter paper (pore size 0.45 μm) to form an interwoven mat of nanowires. After repeated washes with toluene, the filter paper-supported membrane was dried in an oven at 50 ℃ for 30 min before using.

Stability Tests: For water stability testing, all composite membranes were immersed in de-ionized water at room temperature for different times before PL measurement. For photostability tests, the membranes were subjected to UV light irradiation (365 nm, 0.5 $W \cdot cm^{-2}$) at room temperature. The aged samples were then subjected to further characterization. To measure thermal stability, the membranes were placed on a heating plate for several heating/cooling cycles (room temperature/120 °C), after which PL intensities were recorded. Composite membranes were also immersed in boiling water for 60s and cooled down to room temperature for further characterization. To test the stability towards ion-exchange, all composites membranes were immersed in a chloride or iodide solution at room temperature, 80 ℃ or under UV light illumination (365 nm, 0.5 $W \cdot cm^{-2}$) at different times.

Characterization Methods: X-Ray photoelectron spectroscopy (XPS) measurement for elemental composition was conducted on an AXIS ULTRA (England, KRATOS ANALYTICAL Ltd) using an Al mono Kα X-ray source (1486.6 eV) operated at 150 W. PXRD data were acquired using a Bruker AXS D8 Discover X-Ray Diffractometer at a wavelength of Cu K (1.79 Å). FTIR spectrometer for the chemical structures were collected using a Tensor 27 of Bruker Optics. Ultraviolet and visible absorption (UV-vis) spectra of colloidal solutions were collected using a Cary 5000 UV-Vis-NIR spectrophotometer. Fluorescence spectra and absolute PLQYs were collected using an integrated sphere on an Edinburgh Instruments FLS920 spectrophotometer. SEM images were acquired on a JEOL 7800F Field Emission Scanning Electron Microscope, with an EDS mapping system for elemental x-ray analysis. TEM and high-resolution TEM (HR-TEM) data were acquired on a FEI G_2F_{30} electron microscope operated at 200 kV with a Gatan SC 200 CCD camera. The surface contact angle measurements were conducted at 25 °C on an OCA-20

DataPhysics Instruments GmbH with SCA 20 software. The results were based on the average of at least five measurements.

Supporting Information Available

TEM, STEM, SEM, XPS, SEM-EDS and PL of $CsPbBr_3$@CA-SiO_2, $CsPbBr_3$@A-SiO_2 and $CsPbBr_3$/C-SiO_2; The optical photographs of *in situ* growth process of $CsPbBr_3$@CA-SiO_2 over times; The stability test of free NCs and $CsPbBr_3$@CA-SiO_2 membranes in water and under UV illumination. Anion exchange experiments of free $CsPbX_3$ and $CsPbBr_3$@CA-SiO_2 membranes. This material is available free of charge via the Internet at http://pubs.acs.org.

AUTHOR INFORMATION
Corresponding Author
*Email: heling@mail.xjtu.edu.cn
*Email: yliu@lbl.gov
Author Contributions
All authors have given approval to the final version of the manuscript.
Notes
The authors declare no competing financial interest.
ACKNOWLEDGMENT

This work was supported by the National Natural Science Foundation of China (NSFC Grants 51802254, 51573145), the China Postdoctoral Science Foundation Funded Project (2017M623149), the Fundamental Research Funds for the Central Universities (xjj2018053) and Shaanxi province Youth Foundation (2018JQ5011). Materials analysis was also supported by the U.S. Department of Energy, Office of Science, Office of Basic Energy Sciences, Materials Sciences and Engineering Division, under Contract No. DE-AC02-05-CH11231 within the Inorganic/Organic Nanocomposites Program (KC3104) (MJ and YL). Work at the Molecular Foundry was supported by the Office of Science, Office of Basic Energy Sciences, of the U.S. Department of Energy under Contract No. DE-AC02-05CH11231. The authors wish to express their gratitude to the MOE Key Laboratory for Nonequilibrium Condensed Matter and Quantum Engineering of Xi'an Jiaotong University. The authors also thank Jiao Li at Instrument Analysis

Center of Xi'an Jiaotong University for their assistance with TEM analysis. The authors kindly thank Guijiang Zhou and Shujiang Ding in Xi'an Jiaotong University for useful discussions.

REFERENCES

(1) Kovalenko, M. V.; Protesescu, L.; Bodnarchuk, M. I., Properties and Potential Optoelectronic Applications of Lead Halide Perovskite Nanocrystals. *Science* **2017,** *358*, 745-750.

(2) Guner, T.; Demir, M. M., A Review on Halide Perovskites as Color Conversion Layers in White Light Emitting Diode Applications. *Phys. Status Solidi A* **2018,** *215*, 1800120-1800130.

(3) Protesescu, L.; Yakunin, S.; Bodnarchuk, M. I.; Krieg, F.; Caputo, R.; Hendon, C. H.; Yang, R. X.; Walsh, A.; Kovalenko, M. V., Nanocrystals of Cesium Lead Halide Perovskites ($CsPbX_{(3)}$, X = Cl, Br, and I): Novel Optoelectronic Materials Showing Bright Emission with Wide Color Gamut. *Nano Lett.* **2015,** *15*, 3692-3696.

(4) Akkerman, Q. A.; D'Innocenzo, V.; Accornero, S.; Scarpellini, A.; Petrozza, A.; Prato, M.; Manna, L., Tuning the Optical Properties of Cesium Lead Halide Perovskite Nanocrystals by Anion Exchange Reactions. *J. Am. Chem. Soc.* **2015,** *137*, 10276-10281.

(5) Swarnkar, A.; Chulliyil, R.; Ravi, V. K.; Irfanullah, M.; Chowdhury, A.; Nag, A., Colloidal $CsPbBr_3$ Perovskite Nanocrystals: Luminescence beyond Traditional Quantum Dots. *Angew. Chem. Int. Ed. Engl.* **2015,** *54*, 15424-15428.

(6) Bekenstein, Y.; Koscher, B. A.; Eaton, S. W.; Yang, P.; Alivisatos, A. P., Highly Luminescent Colloidal Nanoplates of Perovskite Cesium Lead Halide and Their Oriented Assemblies. *J. Am. Chem. Soc.* **2015,** *137*, 16008-16011.

(7) Yakunin, S.; Protesescu, L.; Krieg, F.; Bodnarchuk, M. I.; Nedelcu, G.; Humer, M.; De Luca, G.; Fiebig, M.; Heiss, W.; Kovalenko, M. V., Low-threshold Amplified Spontaneous Emission and Lasing from Colloidal Nanocrystals of Caesium Lead Halide Perovskites. *Nat. Commun.* **2015,** *6*, 8056-8063.

(8) Pan, J.; Quan, L. N.; Zhao, Y.; Peng, W.; Murali, B.; Sarmah, S. P.; Yuan, M.; Sinatra, L.; Alyami, N. M.; Liu, J.; Yassitepe, E.; Yang, Z.; Voznyy, O.; Comin, R.; Hedhili, M. N.; Mohammed, O. F.; Lu, Z. H.; Kim, D. H.; Sargent, E. H.; Bakr, O. M., Highly Efficient Perovskite-Quantum-Dot Light-Emitting Diodes by Surface Engineering. *Adv. Mater.* **2016,** *28*, 8718-8725.

(9) Veldhuis, S. A.; Boix, P. P.; Yantara, N.; Li, M.; Sum, T. C.; Mathews, N.; Mhaisalkar, S. G., Perovskite Materials for Light-Emitting Diodes and Lasers. *Adv. Mater.* **2016,** *28*, 6804-6834.

(10) Eaton, S. W.; Lai, M.; Gibson, N. A.; Wong, A. B.; Dou, L.; Ma, J.; Wang, L. W.; Leone, S.

R.; Yang, P., Lasing in Robust Cesium Lead Halide Perovskite Nanowires. *Proc. Natl. Acad. Sci.* **2016,** *113*, 1993-1998.

(11) Cho, H.; Kim, Y. H.; Wolf, C.; Lee, H. D.; Lee, T. W., Improving the Stability of Metal Halide Perovskite Materials and Light-Emitting Diodes. *Adv. Mater.* **2018,** 1704587-1704610.

(12) Wang, H. C.; Bao, Z.; Tsai, H. Y.; Tang, A. C.; Liu, R. S., Perovskite Quantum Dots and Their Application in Light-Emitting Diodes. *Small* **2018,** *14*, 1702433-1702455.

(13) Leijtens, T.; Eperon, G. E.; Noel, N. K.; Habisreutinger, S. N.; Petrozza, A.; Snaith, H. J., Stability of Metal Halide Perovskite Solar Cells. *Adv. Energy Mater.* **2015,** *5*, 1500963-1500985.

(14) Chen, J.; Liu, D.; Al-Marri, M. J.; Nuuttila, L.; Lehtivuori, H.; Zheng, K., Photo-stability of $CsPbBr_3$ Perovskite Quantum Dots for Optoelectronic Application. *Sci. China Mater.* **2016,** *59*, 719-727.

(15) Pan, A.; Wang, J.; Jurow, M. J.; Jia, M.; Liu, Y.; Wu, Y.; Zhang, Y.; He, L.; Liu, Y., General Strategy for the Preparation of Stable Luminous Nanocomposite Inks Using Chemically Addressable $CsPbX_3$ Peroskite Nanocrystals. *Chem. Mater.* **2018,** *30*, 2771-2780.

(16) De Roo, J.; Ibanez, M.; Geiregat, P.; Nedelcu, G.; Walravens, W.; Maes, J.; Martins, J. C.; Van Driessche, I.; Kovalenko, M. V.; Hens, Z., Highly Dynamic Ligand Binding and Light Absorption Coefficient of Cesium Lead Bromide Perovskite Nanocrystals. *ACS Nano* **2016,** *10*, 2071-2081.

(17) Kim, Y.; Yassitepe, E.; Voznyy, O.; Comin, R.; Walters, G.; Gong, X.; Kanjanaboos, P.; Nogueira, A. F.; Sargent, E. H., Efficient Luminescence from Perovskite Quantum Dot Solids. *ACS Appl. Mater. Interfaces* **2015,** *7*, 25007-25013.

(18) Raja, S. N.; Bekenstein, Y.; Koc, M. A.; Fischer, S.; Zhang, D.; Lin, L.; Ritchie, R. O.; Yang, P.; Alivisatos, A. P., Encapsulation of Perovskite Nanocrystals into Macroscale Polymer Matrices: Enhanced Stability and Polarization. *ACS Appl. Mater. Interfaces* **2016,** *8*, 35523-35533.

(19) Parobek, D.; Dong, Y.; Qiao, T.; Rossi, D.; Son, D. H., Photoinduced Anion Exchange in Cesium Lead Halide Perovskite Nanocrystals. *J. Am. Chem. Soc.* **2017,** *139*, 4358-4361.

(20) Huang, S.; Li, Z.; Wang, B.; Zhu, N.; Zhang, C.; Kong, L.; Zhang, Q.; Shan, A.; Li, L., Morphology Evolution and Degradation of $CsPbBr_3$ Nanocrystals under Blue Light-Emitting Diode Illumination. *ACS Appl. Mater. Interfaces* **2017,** *9*, 7249-7258.

(21) Wang, Y.; Li, X.; Sreejith, S.; Cao, F.; Wang, Z.; Stuparu, M. C.; Zeng, H.; Sun, H., Photon Driven Transformation of Cesium Lead Halide Perovskites from Few-Monolayer Nanoplatelets to Bulk Phase. *Adv. Mater.* **2016,** *28*, 10637-10643.

(22) Dang, Z.; Shamsi, J.; Palazon, F.; Imran, M.; Akkerman, Q. A.; Park, S.; Bertoni, G.; Prato, M.; Brescia, R.; Manna, L., In Situ Transmission Electron Microscopy Study of Electron Beam-Induced Transformations in Colloidal Cesium Lead Halide Perovskite Nanocrystals. *ACS Nano* **2017,** *11*, 2124-2132.

(23) Nedelcu, G.; Protesescu, L.; Yakunin, S.; Bodnarchuk, M. I.; Grotevent, M. J.; Kovalenko, M. V., Fast Anion-Exchange in Highly Luminescent Nanocrystals of Cesium Lead Halide Perovskites ($CsPbX_3$, X = Cl, Br, I). *Nano Lett.* **2015,** *15*, 5635-5640.

(24) Chang, S.; Bai, Z.; Zhong, H., In Situ Fabricated Perovskite Nanocrystals: A Revolution in Optical Materials. *Adv. Opt. Mater.* **2018**, *6*, 1800380-1800398.

(25) Sun, H.; Yang, Z.; Wei, M.; Sun, W.; Li, X.; Ye, S.; Zhao, Y.; Tan, H.; Kynaston, E. L.; Schon, T. B.; Yan, H.; Lu, Z. H.; Ozin, G. A.; Sargent, E. H.; Seferos, D. S., Chemically Addressable Perovskite Nanocrystals for Light-Emitting Applications. *Adv. Mater.* **2017,** *29*, 1701153-1701161.

(26) Ruan, L.; Shen, W.; Wang, A.; Zhou, Q.; Zhang, H.; Deng, Z., Stable and Conductive Lead Halide Perovskites Facilitated by X-type Ligands. *Nanoscale* **2017,** *9*, 7252-7259.

(27) González-Pedro, V.; Veldhuis, S. A.; Begum, R.; Bañuls, M. J.; Bruno, A.; Mathews, N.; Mhaisalkar, S.; Maquieira, Á., Recovery of Shallow Charge-Trapping Defects in $CsPbX_3$ Nanocrystals through Specific Binding and Encapsulation with Amino-Functionalized Silanes. *ACS Energy Lett.* **2018,** *3*, 1409-1414.

(28) Sun, C.; Zhang, Y.; Ruan, C.; Yin, C.; Wang, X.; Wang, Y.; Yu, W. W., Efficient and Stable White LEDs with Silica-Coated Inorganic Perovskite Quantum Dots. *Adv. Mater.* **2016,** *28*, 10088-10094.

(29) Luo, B.; Pu, Y. C.; Lindley, S. A.; Yang, Y.; Lu, L.; Li, Y.; Li, X.; Zhang, J. Z., Organolead Halide Perovskite Nanocrystals: Branched Capping Ligands Control Crystal Size and Stability. *Angew. Chem. Int. Ed. Engl.* **2016,** *55*, 8864-8868.

(30) Huang, H.; Chen, B.; Wang, Z.; Hung, T. F.; Susha, A. S.; Zhong, H.; Rogach, A. L., Water Resistant $CsPbX_3$ Nanocrystals Coated with Polyhedral Oligomeric Silsesquioxane and Their Use as Solid State Luminophores in All-perovskite White Light-emitting Devices. *Chem. Sci.* **2016,** *7*, 5699-5703.

(31) Pan, J.; Shang, Y.; Yin, J.; De Bastiani, M.; Peng, W.; Dursun, I.; Sinatra, L.; El-Zohry, A. M.; Hedhili, M. N.; Emwas, A. H.; Mohammed, O. F.; Ning, Z.; Bakr, O. M., Bidentate Ligand-Passivated $CsPbI_3$ Perovskite Nanocrystals for Stable Near-Unity Photoluminescence Quantum

Yield and Efficient Red Light-Emitting Diodes. *J. Am. Chem. Soc.* **2018,** *140*, 562-565.
(32) Xuan, T.; Yang, X.; Lou, S.; Huang, J.; Liu, Y.; Yu, J.; Li, H.; Wong, K. L.; Wang, C.; Wang, J., Highly Stable $CsPbBr_3$ Quantum Dots Coated with Alkyl Phosphate for White light-emitting Diodes. *Nanoscale* **2017,** *9*, 15286-15290.
(33) Pan, A.; Jurow, M. J.; Qiu, F.; Yang, J.; Ren, B.; Urban, J. J.; He, L.; Liu, Y., Nanorod Suprastructures from a Ternary Graphene Oxide-Polymer-$CsPbX_3$ Perovskite Nanocrystal Composite That Display High Environmental Stability. *Nano Lett.* **2017,** *17*, 6759-6765.
(34) Loiudice, A.; Saris, S.; Oveisi, E.; Alexander, D. T. L.; Buonsanti, R., $CsPbBr_3$ QD/AlO_x Inorganic Nanocomposites with Exceptional Stability in Water, Light, and Heat. *Angew. Chem. Int. Ed. Engl.* **2017,** *56*, 10696-10701.
(35) Sun, J.-Y.; Rabouw, F. T.; Yang, X.-F.; Huang, X.-Y.; Jing, X.-P.; Ye, S.; Zhang, Q.-Y., Facile Two-Step Synthesis of All-Inorganic Perovskite $CsPbX_3$ (X = Cl, Br, and I) Zeolite-Y Composite Phosphors for Potential Backlight Display Application. *Adv. Funct. Mater.* **2017,** *27*, 1704371-1704378.
(36) Li, X.; Wang, Y.; Sun, H.; Zeng, H., Amino-Mediated Anchoring Perovskite Quantum Dots for Stable and Low-Threshold Random Lasing. *Adv. Mater.* **2017,** *29*, 1701185-1701193.
(37) Wei, Y.; Deng, X.; Xie, Z.; Cai, X.; Liang, S.; Ma, P. a.; Hou, Z.; Cheng, Z.; Lin, J., Enhancing the Stability of Perovskite Quantum Dots by Encapsulation in Crosslinked Polystyrene Beads via a Swelling-Shrinking Strategy toward Superior Water Resistance. *Adv. Funct. Mater.* **2017,** *27*, 1703535-1703542.
(38) Zhong, Q.; Cao, M.; Hu, H.; Yang, D.; Chen, M.; Li, P.; Wu, L.; Zhang, Q., One-Pot Synthesis of Highly Stable $CsPbBr_3$@SiO_2 Core-Shell Nanoparticles. *ACS Nano* **2018**, *12*, 8579-8587.
(39) Yuan, S.; Chen, D.; Li, X.; Zhong, J.; Xu, X., In Situ Crystallization Synthesis of $CsPbBr_3$ Perovskite Quantum Dot-Embedded Glasses with Improved Stability for Solid-State Lighting and Random Upconverted Lasing. *ACS Appl. Mater. Interfaces* **2018,** *10*, 18918-18926.
(40) Wang, Y.; He, J.; Chen, H.; Chen, J.; Zhu, R.; Ma, P.; Towers, A.; Lin, Y.; Gesquiere, A. J.; Wu, S. T.; Dong, Y., Ultrastable, Highly Luminescent Organic-Inorganic Perovskite-Polymer Composite Films. *Adv. Mater.* **2016,** *28*, 10710-10717.
(41) Hai, J.; Li, H.; Zhao, Y.; Chen, F.; Peng, Y.; Wang, B., Designing of Blue, Green, and Red $CsPbX_3$ Perovskite-codoped Flexible Films with Water Resistant Property and Elimination of Anion-exchange for Tunable White Light Emission. *Chem. Commun.* **2017,** *53*, 5400-5403.

(42) Hou, S.; Guo, Y.; Tang, Y.; Quan, Q., Synthesis and Stabilization of Colloidal Perovskite Nanocrystals by Multidentate Polymer Micelles. *ACS Appl. Mater. Interfaces* **2017,** *9*, 18417-18422.

(43) Lou, S.; Xuan, T.; Yu, C.; Cao, M.; Xia, C.; Wang, J.; Li, H., Nanocomposites of $CsPbBr_3$ Perovskite Nanocrystals in an Ammonium Bromide Framework with Enhanced Stability. *J. Mater. Chem. C* **2017,** *5*, 7431-7435.

(44) Wu, Y.; Wei, C.; Li, X.; Li, Y.; Qiu, S.; Shen, W.; Cai, B.; Sun, Z.; Yang, D.; Deng, Z.; Zeng, H., In Situ Passivation of $PbBr_6^{4-}$ Octahedra toward Blue Luminescent $CsPbBr_3$ Nanoplatelets with Near 100% Absolute Quantum Yield, *ACS Energy Lett.* **2018**, *3*, 2030-2037

(45) Li, X.; Wu, Y.; Zhang, S.; Cai, B.; Gu, Y.; Song, J.; Zeng, H., $CsPbX_3$ Quantum Dots for Lighting and Displays: Room-Temperature Synthesis, Photoluminescence Superiorities, Underlying Origins and White Light-Emitting Diodes, *Adv. Funct. Mater.* **2016**, *26*, 2435-2445(46) Chen, D.; Yuan, S.; Chen, X.; Li, J.; Mao, Q.; Li, X.; Zhong, J., $CsPbX_3$ (X = Br, I) Perovskite Quantum Dot Embedded Low-melting Phosphosilicate Glasses: Controllable Crystallization, Thermal Stability and Tunable Emissions. *J. Mater. Chem. C* **2018,** *6*, 6832-6839.

(47) Yi, D.; Xu, C.; Tang, R.; Zhang, X.; Caruso, F.; Wang, Y., Synthesis of Discrete Alkyl-Silica Hybrid Nanowires and Their Assembly into Nanostructured Superhydrophobic Membranes. *Angew. Chem. Int. Ed. Engl.* **2016,** *55*, 8375-8380.